A Numerical Study of Stably Stratified Flow Past a Sphere

Zhao Zhang, Joanna Szmelter, Piotr K. Smolarkiewicz

Synopsis

Stably stratified flows past a 3D sphere and a hemisphere are simulated using a new non-oscillatory forward-in-time (NFT) anelastic unstructured-mesh flow solver that accounts for both laminar and turbulent boundary layers.

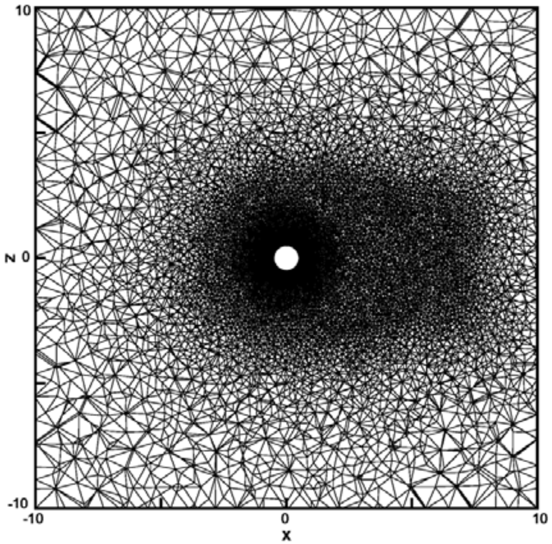

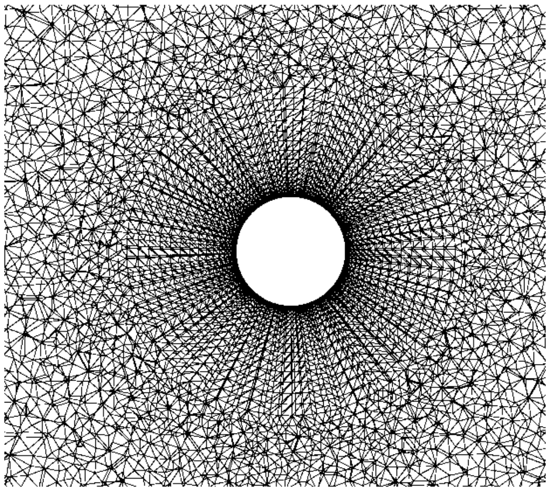

Fig. 1: The $y = 0$ cross-section of the primary 3D hybrid mesh, consisting of prismatic layers around the sphere and tetrahedral elements elsewhere. The left panel shows the mesh over the whole domain, while the right panel shows the prismatic layers around the sphere.

Stably Stratified flow past a sphere with laminar boundary layers

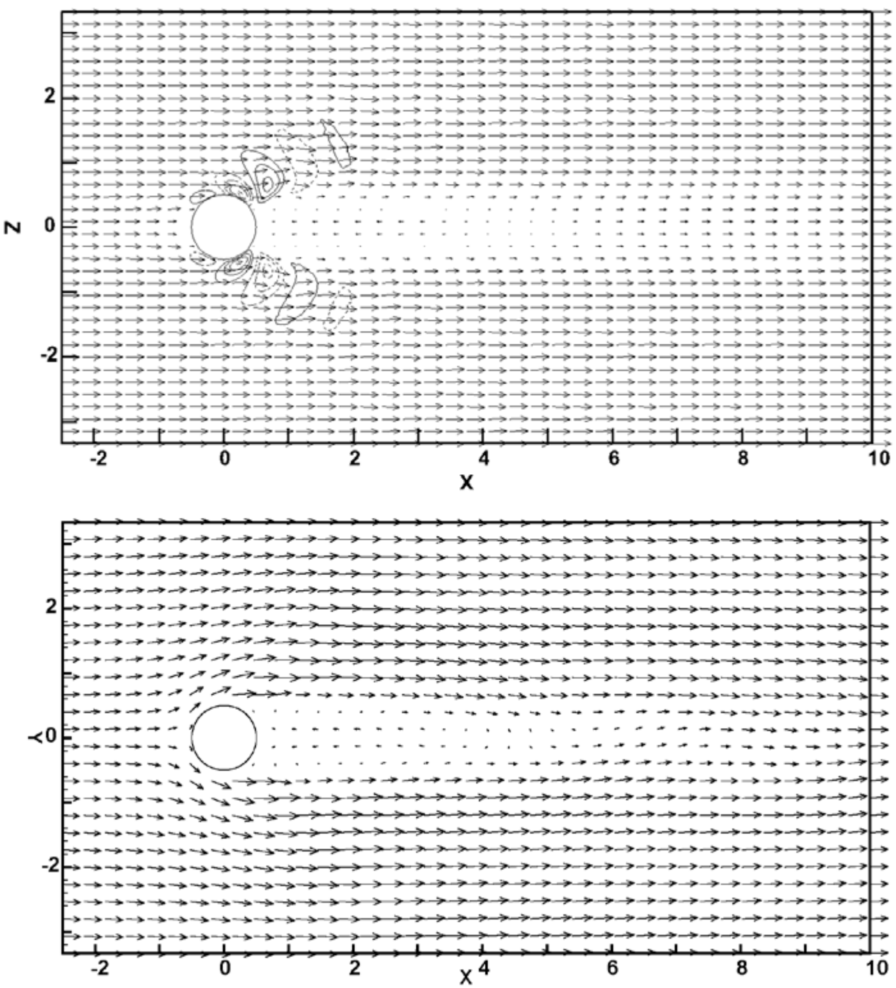

Fig.2 Vertical velocity isolines in $y = 0$ plane (top) and $y = 0$ plane (bottom), for $Fr = 0.4$ and $Re = 200$.

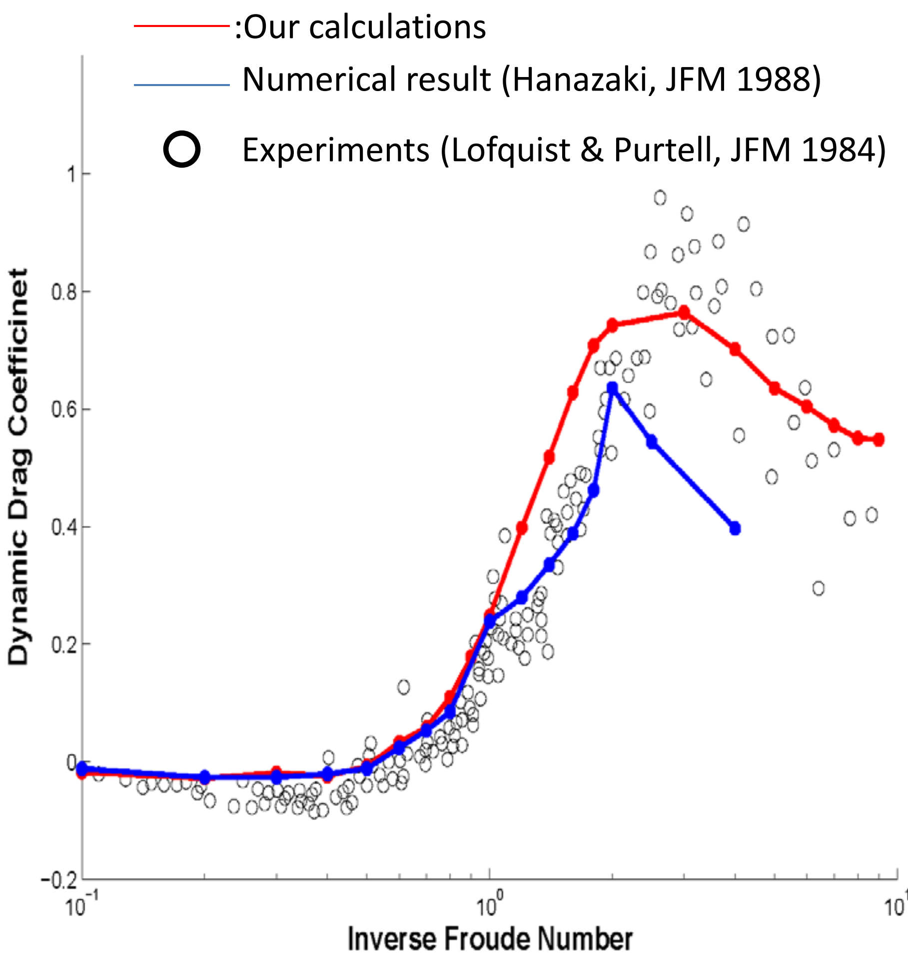

Fig. 3 The dynamic drag coefficient, ΔC_d=$C_d\left(Re, \frac{1}{Fr}\right) - C_d(Re, 0)$, for $Re = 200$ and $1/\mathrm{Fr} = 0.1$ to 9.0 .

A Numerical Study of Stably Stratified Flow Past a Sphere

Zhao Zhang[1], *Joanna Szmelter*[2], *Piotr K. Smolarkiewicz*[3]

Numerical Method

A study is reported that examines simulations of stratified three-dimensional flow past a sphere and a hemisphere for a range of stable stratifications, and both laminar and turbulent boundary layer flows.

A non-oscillatory forward-in-time (NFT) nonhydrostatic unstructured-mesh flow solver is employed to integrate inhomogeneous transport equations, $\frac{\partial \psi}{\partial t} = -div(\boldsymbol{v}\psi) + R$, according to

$$\psi_i^{n+1} = A_i\left(\psi^n + 0.5\delta t R^n, \boldsymbol{v}^{n+\frac{1}{2}}\right) + 0.5\delta t R_i^{n+1},$$

where A denotes the Multi-dimensional Positive Definite Advection Transport Algorithm (MPDATA) [4], and ψ_i^{n+1} is the solution sought at the node i of a co-located mesh at time step $n+1$. .

Discretization

The spatial discretisation uses the edge-based median-dual finite volume approach, integrating the generic physical form of the governing PDE over arbitrarily-shaped cells.

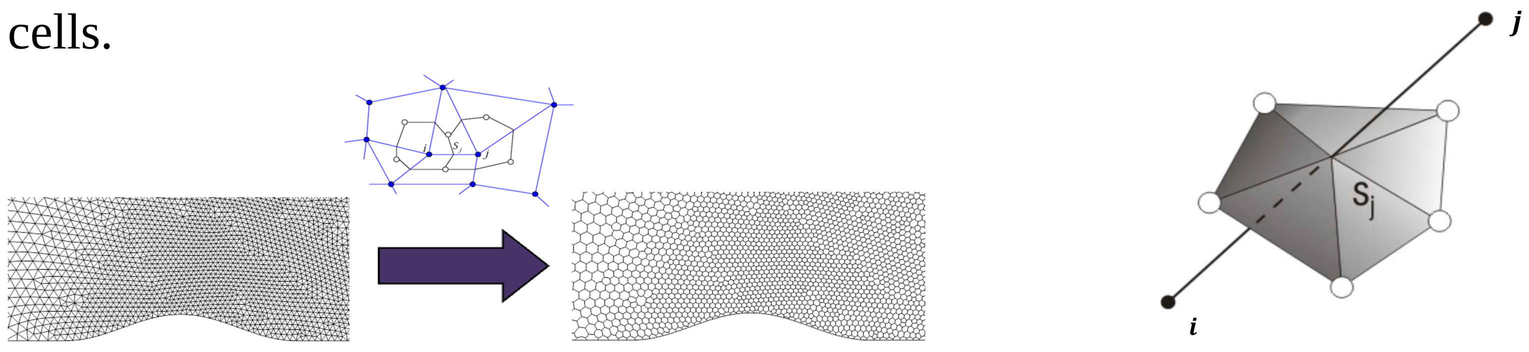

The edge-based median-dual approach in 3D. The edge connecting vertices i and j of the primary mesh pierces (at the edge centre) the face S_j of a computational dual cell surrounding vertex i.

Figure 1: The edge-based median-dual approach in 2D (left) and 3D (right).

Stratified laminar Flow Past a Sphere

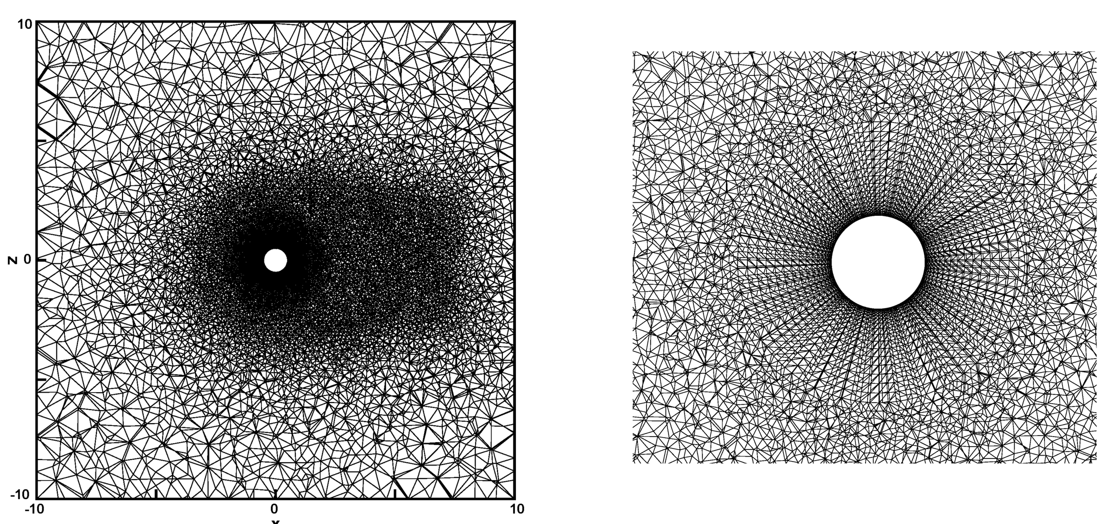

Figure 2: The $y = 0$ cross-section of the primary 3D hybrid mesh, consisting of prismatic layers around the sphere and tetrahedral elements elsewhere. The left panel shows the mesh over the whole domain, while the right panel shows the prismatic layers around the sphere.

A sphere of radius $a = 0.5$ is placed in the centre of the $20 \times 20 \times 20$ domain; see Fig. 2. The incompressbile Boussinesq option of the anelastic model [4] is adopted. The Reynolds number ($Re = 2\rho U a/\mu$) is 200 and the Froude number ($Fr = U/Na$) varies from 0.1 to 200, and $+\infty$.

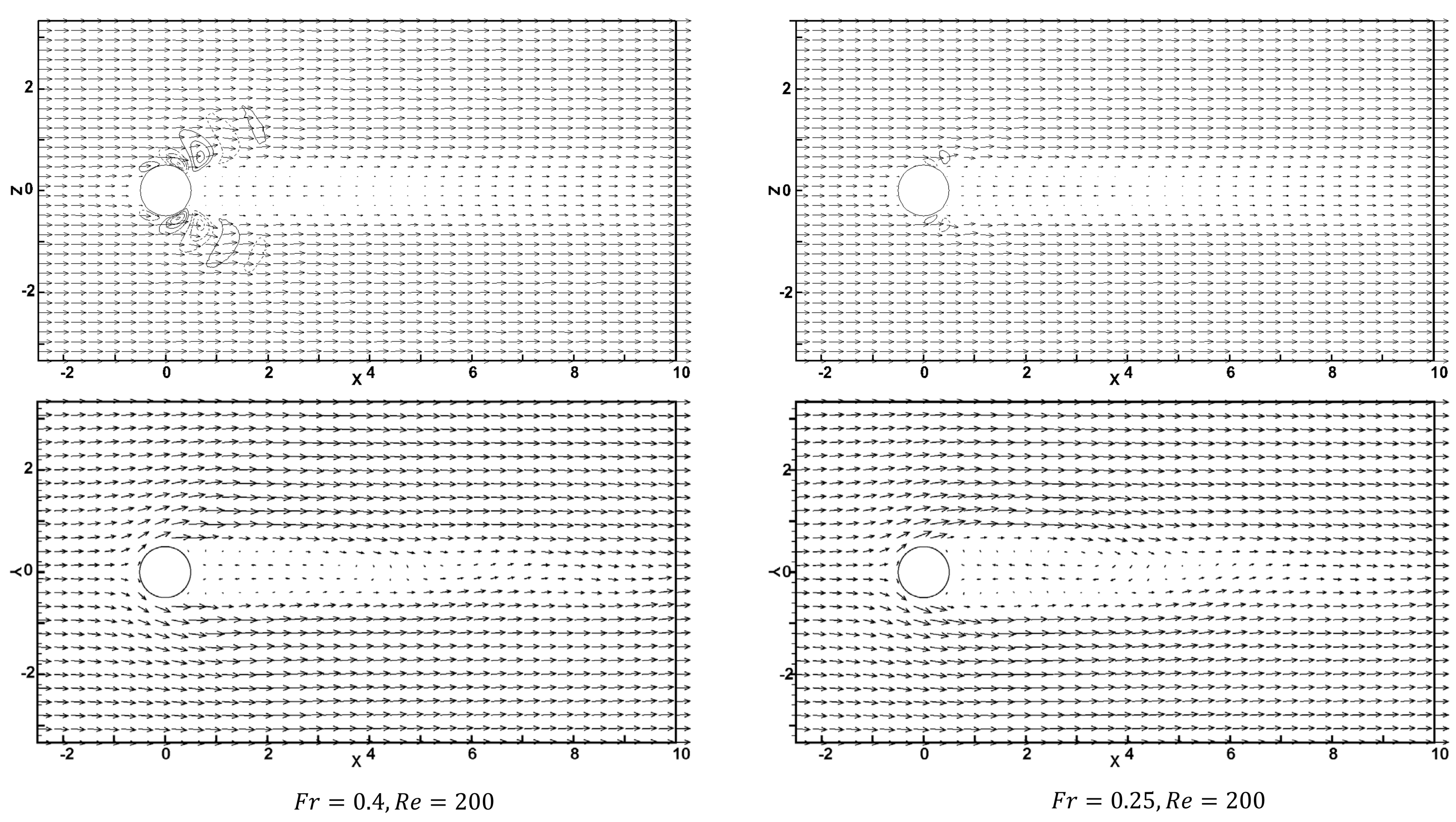

Figure 3: Vertical velocity isolines in $y = 0$ plane (top) and $z = 0$ plane (bottom) for selected Froude numbers; positive and negative values are plotted with solid and dashed lines, respectively. Representative velocity vectors are also shown. These solutions compare well with corresponding numerical and laboratory results in [1] and [2].

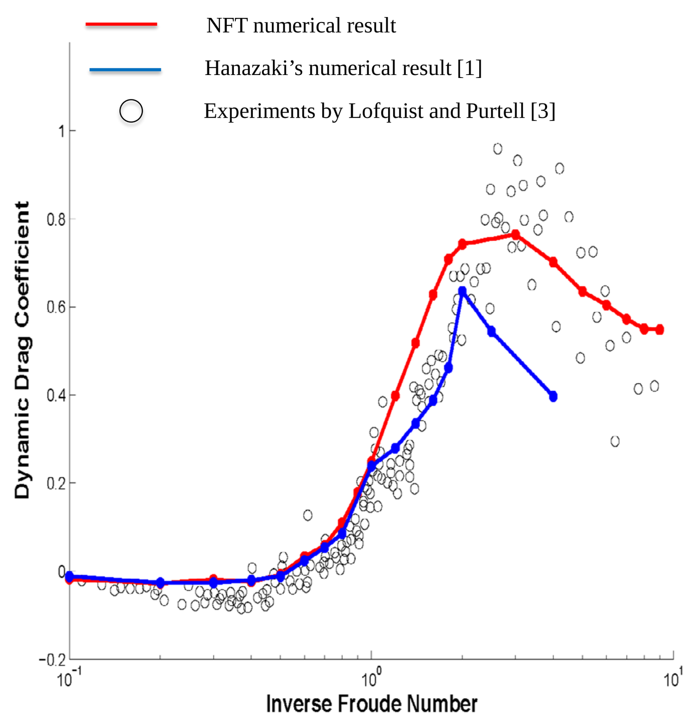

Figure 4: The dynamic drag coefficient, $\Delta C_d = C_d\left(Re, \frac{1}{Fr}\right) - C_d(Re, 0)$, for $Re = 200$ and $1/\mathrm{Fr} = 0.1$ to 9.0 .

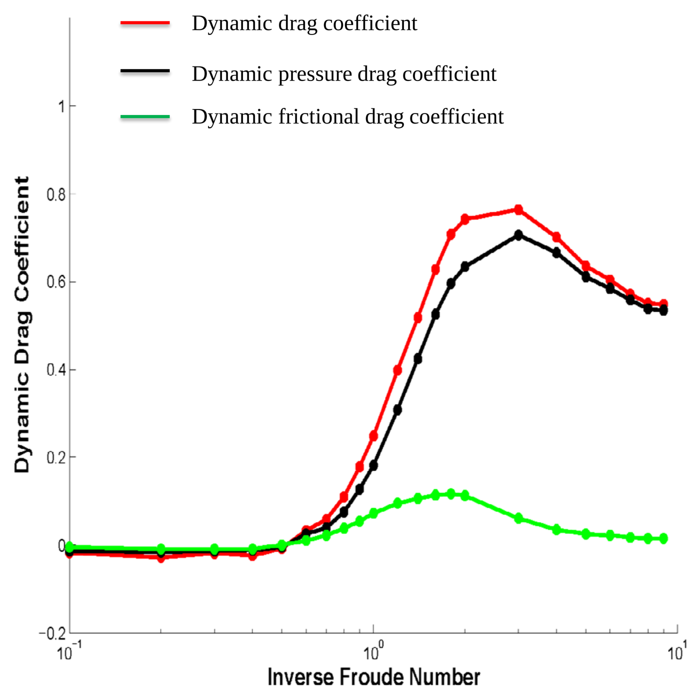

Figure 5: The dynamic drag coefficient as the sum of pressure and frictional drag; cf. Fig. 9 in [1].

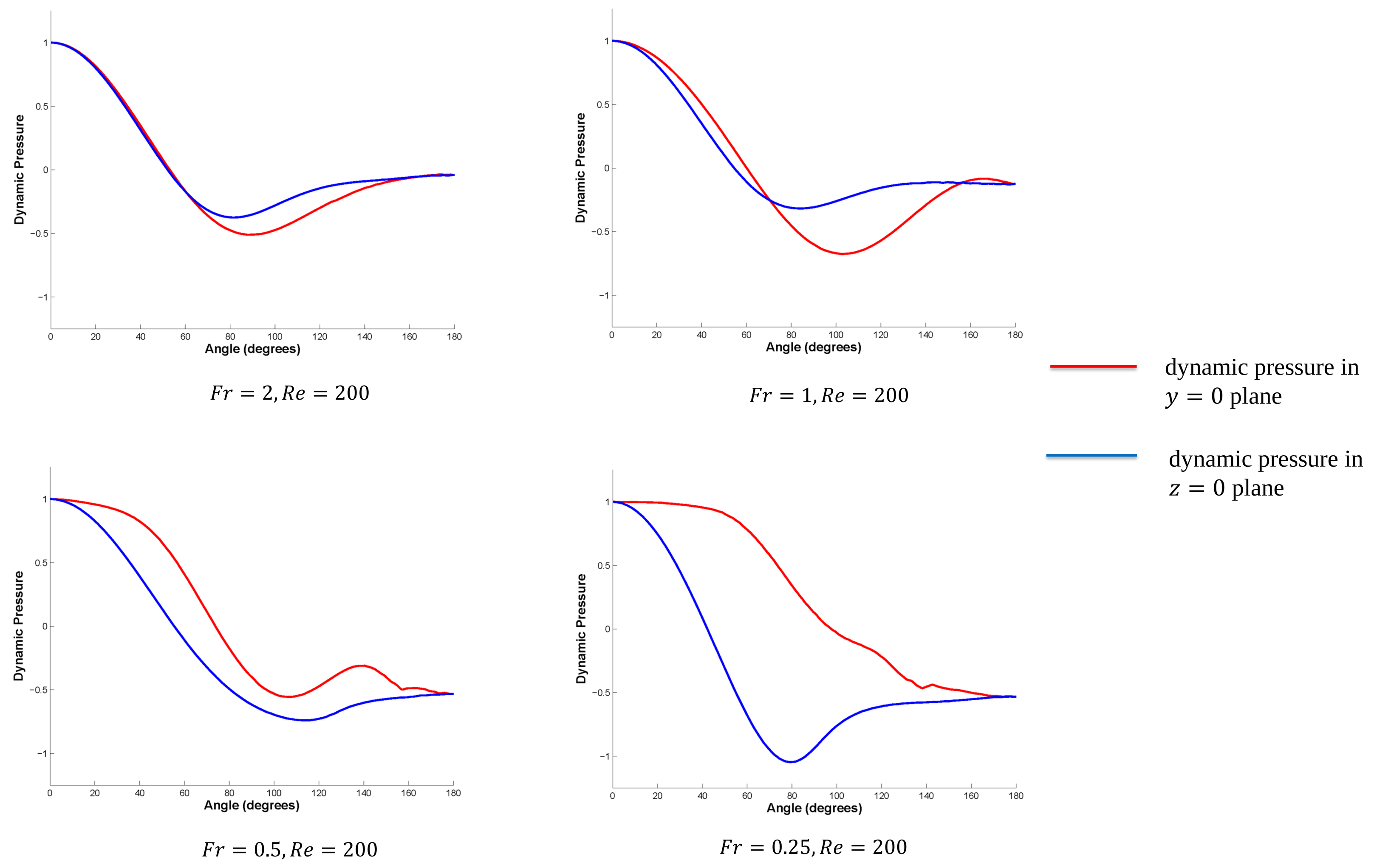

Figure 6: Dynamic pressure distribution on the sphere's surface. Red and blue curves correspond to $y = 0$ and $z = 0$ planes shown in Fig. 3; cf. Figure 4 in [1]. The angle is measured from the upstream stagnation point.

Stratified Turbulent Flow Past a Sphere and a Hemi-sphere

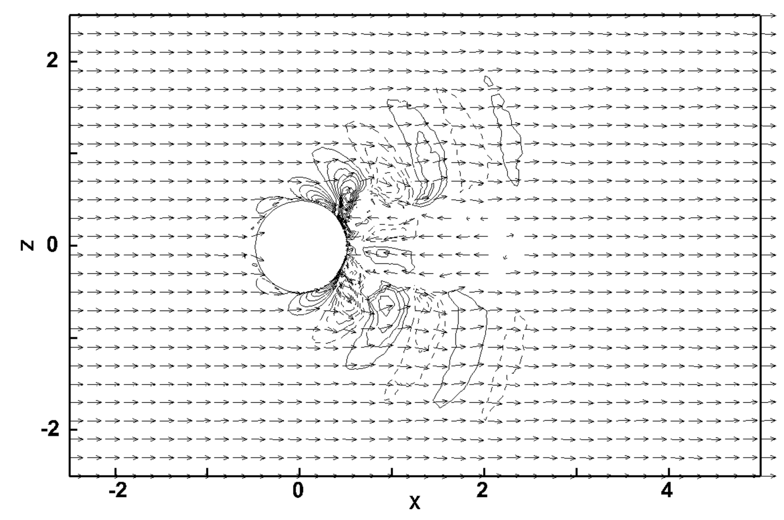

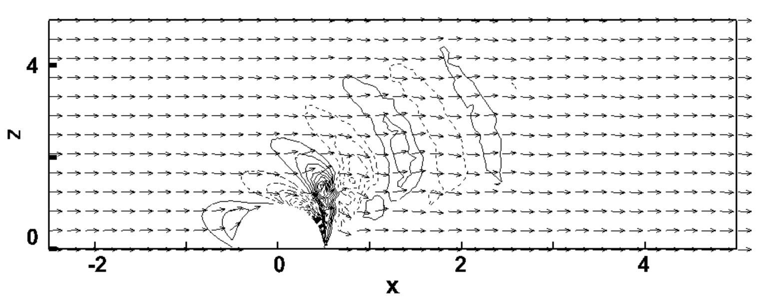

Figure 7: $Re \to +\infty$ and $Fr = 1/3$ flows past the sphere (top) and the hemisphere (bottom) in $y = 0$ planes. Isoline values are the same as in Fig. 3.

Remarks

- Stronger stratification leads to weaker lee-waves, and a laminar boundary layer tends to suppress wave motions in the lee.
- Our NFT numerical values of the drag coefficient compare well with experimental results in [3], but for $Fr > 1$ differ from numerical results in [1].
- The lee-flow patterns past a sphere and a hemisphere are different. For the sphere case, the near-field lee-flow is directed backwards; whereas, there is no significant adverse flow in the lee of the hemisphere. This contrasts with simulations of atmospheric low Froude number flows past smooth hills [4].
- The current work demonstrates the skilfulness of our NFT solver for modelling laminar and turbulent stably stratified flows on unstructured meshes, for a range of Froude numbers.

REFERENCES

1. H. Hanazaki, A numerical study of three-dimensional stratified flow past a sphere. J. Fluid. Mech. 192 (1988) 393-419
2. Q. Lin, W. R. Lindberg, D. L. Boyer and H. J. S. Fernando, Stratified flow past a sphere. J. Fluid Mech. 240 (1992) 315-354
3. K. E. B. Lofquist, L. P. Purtell, Drag on a sphere moving horizontally through a stratified liquid. J. Fluid. Mech. 148(1984), 271-284
4. P. K. Smolarkiewicz, J. Szmelter, A. A. Wyszogrodzki , An unstructured-mesh atmospheric model for nonhydrostatic dynamics, J. Comput. Phys. 254 (2013) 184-199

CONTACT INFORMATION

1. Loughborough University Leicestershire LE11 3TU, UK
z.zhang@lboro.ac.uk
2. Loughborough University Leicestershire LE11 3TU, UK
j.szmelter@lboro.ac.uk
3. ECMWF, Shinfield Park, Reading, Berkshire, RG2 9AX, UK
piotr.smolarkiewicz@ecmwf.int